Article

Roles of Salicylate Donors in Enhancement of Productivity and Isotacticity of Ziegler–Natta Catalyzed Propylene Polymerization

Manussada Ratanasak [1], Jun-ya Hasegawa [1] and Vudhichai Parasuk [2,*]

[1]   Institute for Catalysis, Hokkaido University, Kita 21, Nishi 10, Sapporo, Hokkaido 001-0021, Japan;
    manussada@cat.hokudai.ac.jp (M.R.); hasegawa@cat.hokudai.ac.jp (J.-y.H.)
[2]   Center of Excellence in Computational Chemistry, Department of Chemistry, Faculty of Science,
    Chulalongkorn University, Bangkok 10330, Thailand
[*]   Correspondence: vudhichai.p@chula.ac.th; Tel.: +66-2218-7603

check for updates

Abstract: Roles of internal salicylate donors (SID) in enhancing activity and stereoselectivity of Ziegler–Natta catalyzed propylene (PP) polymerization were examined using DFT calculations. Five salicylate donors were studied. The chelate mode is the preferred adsorption mode. The linear relationship ($R^2 = 0.96$) between calculated adsorption energies (E_{ads}) of five SIDs and the experimental PP activities was observed. Thus, the SID with the strongest adsorption energy will provide the highest activity in agreement with our previous studies. Compared with diisobutyl phthalate (DIBP), which is the industrial electron donor, SID has stronger E_{ads}. The insertion step, which involves the π-complex formation (ΔE_π) and the insertion activation or intrinsic activation energy (E_a) for PP polymerization was also examined. The relation between ln(activity) and apparent activation energy (E_a(app)), which is $\Delta E_\pi + E_a$ for the primary(1,2)-*re* insertion with $R^2 = 0.99$, was observed. The salicylate donor also has a lower E_a(app) than that of DIBP. This explains the better catalytic performance of SID. Our results also demonstrated that the size and the type of hydrocarbon substituents play a key role in controlling stereoselectivity and activity. In addition, we found a good relationship between E_{ads} and both intrinsic (E_a) and apparent (E_a(app)) activation energies of five salicylate donors with R^2 of 0.90 and 0.97, respectively.

Keywords: salicylate donor; Ziegler–Natta; propylene polymerization; stereoselectivity

---

1. Introduction

Transition metal-based catalysts for olefin polymerization play a crucial role in the development of novel versatile and environmentally-friendly polymeric materials, including both commodity and specialty polymers [1]. Polypropylene (PP) is among the highest in demand polymer/plastic due to its high-performance characteristics such as high level of stiffness, high melting point compared to other commercial thermoplastics, good resistance to impacts, low production cost, high heat distortion temperature, transparency, and ability to be recycled, etc. [2–4]. Most of the commercial catalysts used for PP manufacture are modified from the original Ziegler–Natta (ZN) system by adding organic Lewis bases or electron donors to enhance productivity and isotacticity [5]. Electron donors, which are added during catalyst preparation, are called internal electron donors and those added during the polymerization process are called external electron donors [6]. Since internal electron donors are mixed with the ZN catalyst during preparation, it strongly impacts the active center of the ZN catalyst and the microstructure of PP. Thus, the internal (electron) donor has become a key component for improving the comprehensive properties of polypropylene [7–9]. Many classes of chemical compounds [10–15] have been employed as internal donors in the ZN-catalyzed propylene polymerization.

Recently, Zhou et al. [16] synthesized five salicylate (SID) compounds with different sizes of hydrocarbon substituents for heterogeneous ZN-catalyzed PP polymerization. They were comprised of isobutyl 2-benzyloxybenzoate (SID-1), isobutyl 2-benzyloxy-3-methyl benzoate (SID-2), isobutyl 2-trimethyloxy-3-methyl benzoate (SID-3), isobutyl 2-benzyloxy-3,5-isopropyl benzoate (SID-4), and isobutyl 2-benzyloxy-3,5-tert-butyl benzoate (SID-5) (see Figure 1, Table 1). These new electron donors are around 2–3 times more effective in enhancing the activity of the ZN catalyst than the industrially used diisobutyl phthalate (DIBP) donor [16].
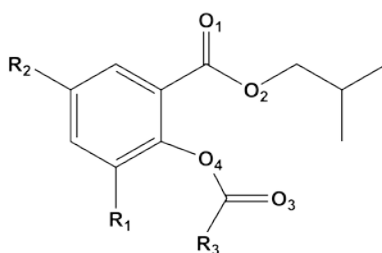

Figure 1. Chemical structure of salicylate donors with different substituent groups at R_1, R_2, and R_3 positions.

Table 1. Salicylate donors (SID) with different substituent groups at R_1, R_2 and R_3 positions and experimental data [16].

SID	R_1	R_2	R_3	Activity (kgPP gTi^{-1})	%mm [a]	%I.I. [b]
SID-1	H	H	Ph	660	85.5	96.3
SID-2	Me	H	*t*Bu	1370	88.1	96.9
SID-3	Me	H	Ph	1030	89.6	98.0
SID-4	*i*Pr	*i*Pr	Ph	2410	91.0	98.6
SID-5	*t*Bu	*t*Bu	Ph	2370	88.9	97.7

[a] %mm denotes the average meso (isotactic) sequence length or % triads of polypropylene from ^{13}C-NMR [16].
[b] %I.I. denotes % of the isotactic index was tested by extraction with boiling *n*-heptane for 6 h [16].

There have been several theoretical studies on roles of electron donors such as malonates [17], succinates [18,19], 1,3-diethers [19–21], phthalates [22,23], methyl benzoates [14,24], ethyl benzoates [25,26], alkoxysilanes [27–29], and dibenzoyl sulfide in ZN-catalyzed PP polymerization [23]. Since salicylate compounds are the newest electron donors, no theoretical study on this topic has been reported. The purpose of this work is, therefore, to understand the roles of salicylate donors in enhancing activity and stereoselectivity of the ZN catalyst. Furthermore, to guide the design of future electron donors obtained results were used to compare with our previous theoretical works on other electron donors, especially with DIBP [23].

Many researchers have shown that Ziegler–Natta catalysts are highly regioselective for PP polymerization [17,23,30–32]. The accepted mechanism for olefin polymerization was given by Cossee and Arlman [33–35] and Brookhart and Green [36]. In principle, the ZN-catalyzed PP polymerization is composed of three steps: insertion, propagation, and termination. The PP insertion is the rate determining step (RDS) [4,37], as well as the stereocontrol step [38]. Thus, the insertion step for ZN-catalyzed PP polymerization with five salicylates as given in Table 1 was investigated. Since the energy of the transition state for the primary (1,2) insertion of propylene to Ti-*i*Bu bond has been reported by several research groups to be lower than that of the secondary (2,1) insertion [17,19,22,23,39]. Therefore, in this work, we considered only the primary (1,2) insertion for the investigation of the roles of salicylate donors in enhancing activity and stereoselectivity of the ZN catalyst.

2. Computational Details

2.1. Adsorption Modes

The [$Mg_{13}Cl_{26}.Cl_2Ti$] cluster was employed for modeling of the pre-activated $MgCl_2$ (110) surface of the ZN catalyst similar to our previous work. [23] The $MgCl_2$ (110) surface model has been proven both experimentally and theoretically to be the most stable plane [40–44]. An octahedral shape of a mononuclear Ti atom adsorbing on the $MgCl_2$ (110) plane is also a good model for the activated catalyst, and this surface model could reproduce experimental Raman spectra of the $MgCl_2$-$TiCl_4$ sample [45].

Four possible adsorption modes, i.e., mono, chelate, bridge, and zip modes, as illustrated in Figure 2, were investigated.

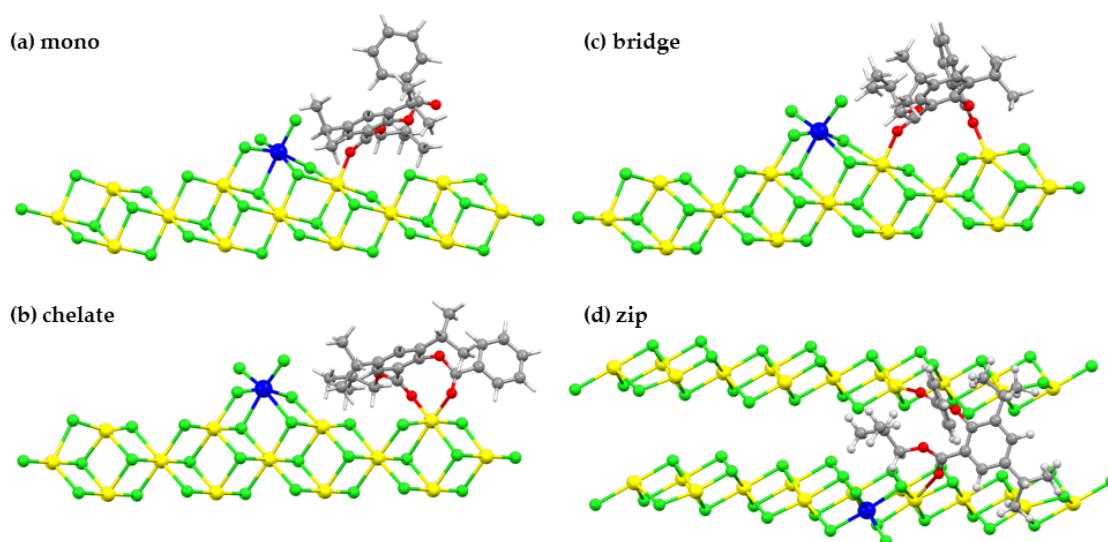**Figure 2.** Four different adsorption modes, (**a**) mono, (**b**) chelate, (**c**) bridge, and (**d**) zip of the salicylate donor (SID-4) on the Ziegler–Natta (ZN) catalyst. Color key: Mg, yellow; Ti, blue; Cl, green; O, red; C, gray; H, white.

Adsorption energies were obtained using DFT calculations with the B3LYP-D3 functional [46]. This functional has been proven by Cavallo et al. [47] to well reproduce the experimental association energies between $TiCl_4$ of fifteen electron donors. The LANL2DZ effective core potentials (ECP) function and basis set were used for Ti atom [48], while the 6-31G(d,p) basis set was used for others. During the optimization of the geometry for the [$Mg_{13}Cl_{26}.Cl_2Ti$] cluster, which represented the $MgCl_2$ (110) surface, the four $MgCl_2$ units at the top layer, which involved donor and Ti coordination, were relaxed. The remaining $MgCl_2$ units were fixed to the $MgCl_2$ X-ray structure [49], while the geometry of donor molecules was fully optimized. The adsorption energy (E_{ads}) is defined according to Equation (1):

$$E_{ads} = E(complex) - E(surface) - E(donor) \tag{1}$$

where E(complex) is the energy of the complex between the electron donor and the $TiCl_4$/$MgCl_2$ (110) surface. E(surface) and E(donor) are the energies of the $TiCl_4$/$MgCl_2$ (110) surface and the electron donor, respectively. All DFT calculations were conducted by employing the Gaussian 09, Revision B.01. program [50].

2.2. Activation Energies and Stereoselectivities

The active surface model was constructed by adding the isobutyl (*i*Bu) group to the Ti center of the complex structure between the [$Mg_{13}Cl_{26}.Cl_2Ti$] cluster and the salicylate donor. The use of *i*Bu as the growing chain followed the suggestion of Tom Ziegler et al., [32]. In their article, methyl, propyl,

isobutyl, and 2-butyl groups were used as the model for growing polymer chains for investigating the influence of the growing polymer chain on stereoselectivity. Their results revealed that the bulkiness of the polymer chain disfavors propylene insertion, and that the 1,2-*re* insertion is the most favorable. Thus, the stereoselectivity is controlled by the interaction between the propylene and the growing polymer chain. Besides, we have considered (+) and (-) orientations of the *i*Bu growing chain according to Corradini's model [51–53]. Possible orientations of *i*Bu within the (+) and (-) growing chain were also considered. Illustrations of six possible conformations of the *i*Bu growing chain for the π-complex of 1,2-*re* and 1,2-*si* insertions in the presence of the salicylate donor (SID-4) are given in Figure 3. The Ti atom has the +3 oxidation state and contains one unpaired electron. Hence, the doublet spin state was set. Spin-unrestricted calculations for the open-shell systems were performed throughout this investigation using the same level of theory as described in Section 2.1. Also, the four MgCl$_2$ units at the top layer, which involved donor and Ti coordination, were relaxed. The remaining MgCl$_2$ units were frozen at the bulk MgCl$_2$ value [54]. The flexible cluster model allows atoms to adjust their positions according to interactions with adsorbed molecules and it has been employed for the active surface of the Ziegler-Natta catalyst in several works [39,42,55]. The genuineness of the transition state was ensured by the presence of one imaginary frequency.
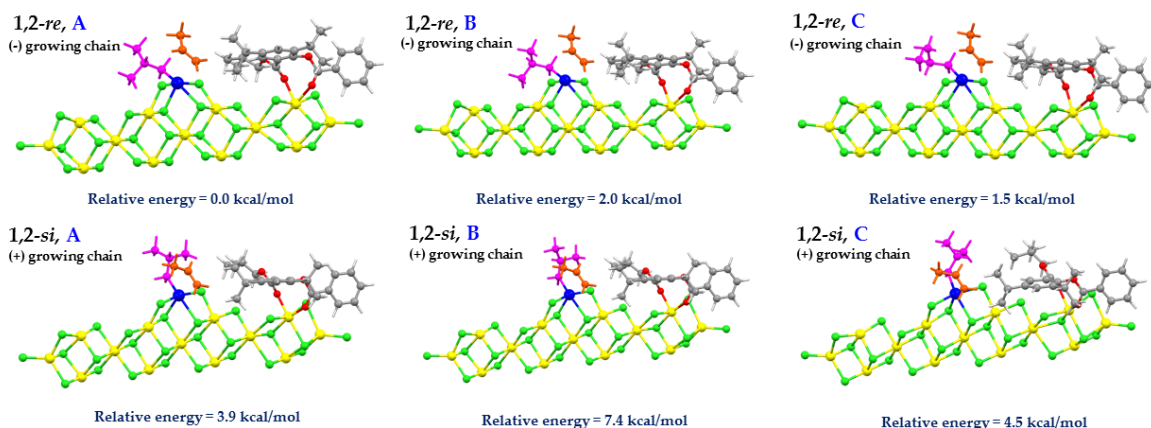

Figure 3. Six possible conformations of the *i*Bu growing chain for the π-complex of 1,2-*re* and 1,2-*si* insertions at the Ti mononuclear on the MgCl$_2$ (110) surface in the presence of salicylate donor (SID-4). The insertion of propylene on the front side, 1,2-*re*, A and 1,2-*si*, A. The insertion of propylene on the backside, 1,2-*re*, B and 1,2-*si*, B. The insertion on propylene on the right side, 1,2-*re*, C and 1,2-*si*, C.

In this study, we focused only on the primary insertion modes, i.e., 1,2-*si* and 1,2-*re*, of propylene monomer into a Ti−*i*Bu. For both enantiofaces, the growing chain is oriented to minimize the steric interactions between the growing chain and the methyl group of the PP monomer. For example, in the case of 1,2-*re* enantioface, the methyl group of the PP monomer is on the opposite side to the growing chain and both methyl on the *i*Bu group avoid the methyl on the PP monomer which gives the least steric repulsion (see Figure 3, 1,2-*re*, A). Therefore, we will use the most stable structure of *i*Bu growing chain conformation with 1,2-*si* and 1,2-*re* of propylene insertions for investigation stereoselectivities and calculated activation energies of five salicylate donors.

3. Results and Discussion

3.1. Preferred Adsorption Modes of Salicylate Donors

Adsorption energies between isobutyl 2-benzyloxy-3,5-isopropyl benzoate or (SID-4) and the model of the pre-activated MgCl$_2$ (110) surface for four adsorption modes, mono, chelate, bridge, and zip were calculated. Their values in kcal/mol together with O-Mg distances in Å were listed in Table 2. The SID-4 was selected to represent the salicylate donor since this compound gave the highest activity in the experiment, see Table 1 [16].

Table 2. Adsorption energies (E_{ads}) and O-Mg distances of salicylate donor (SID-4) adsorbed on the pre-activated $MgCl_2$ (110) surface with four different adsorption modes.

Adsorption Mode	E_{ads} (kcal/mol)	Distance (Å)			
		O_1-Mg	O_2-Mg	O_3-Mg	O_4-Mg
Mono	−30.2	1.99	4.04	4.49	4.41
Chelate	−51.2	2.03	4.17	2.09	3.58
Bridge	−45.9	2.03	3.74	2.06	3.24
Zip	−42.0	5.58	4.06	1.98	4.17

Adsorption energies of the mono, the chelate, the bridge, and the zip coordination modes of the SID-4 adsorbed to the pre-activated $MgCl_2$ (110) surface are −30.2, −51.2 −45.9, and −42.0 kcal/mol, respectively. Thus, the most preferred adsorption mode for salicylate donors is the chelate mode, and the mono mode is the least favorite. The preferential binding mode of the salicylate donor to the $MgCl_2$ (110) surface can be explained. The salicylate donor has two carbonyl oxygen atoms and large substituents. In the mono mode, the electron donor binds to the surface in the nearest vicinity of the titanium atom. Due to the steric repulsion, the mono mode forms the least stable complex, while the two carbonyl oxygens allow the electron donor to form a four-coordination complex with $MgCl_2$ (110) surface that enhances the stability of the chelate mode. Unlike the case of monoester-type electron donors, such as methyl or ethyl benzoate, which have smaller substituents and one carbonyl oxygen, the mono coordination is the most preferred mode [14,26,42]. For the zip coordination, O_1/O_2 to Mg distances are longer than 4 Å. This suggests that the salicylate donor does not bind to the $MgCl_2$ (110) surface. Nevertheless, the salicylate donor used one carbonyl oxygen at the O_3 position bind to the Mg atom of the neighboring adsorption site on the $MgCl_2$ (110) surface to reduce the steric interaction, caused by the large substituents of the donor. For the mono, chelate, and bridge coordination modes, distances between oxygen and Mg atoms are 1.99–2.09 Å for the carbonyl O_1/O_3 and 3.24–4.41 Å for the ether O_2/O_4. For all modes, the average carbonyl O-Mg distance is around 2.0 Å. This is understandable, since not only does the ether oxygen have less electron density (see O_1–O_4 charges in Table S1 in the supporting information), but there is also a strong repulsion between the ether moiety and the surface. However, it should be noted that the adsorption energy of the salicylate donor is irrespective of the coordinated distance.

3.2. Adsorption Energies of Five Salicylate Donors

In the last section, we carried out calculations to investigate the preferred adsorption modes of the salicylate donor. The calculations suggested that the chelate mode is energetically favorable. Therefore, the chelate mode was used as the adsorption mode for calculations of the adsorption energies of five salicylate donors. Adsorption energies (E_{ads}) in kcal/mol and O-Mg distances in Å of the five salicylate donors adsorbed on the pre-activated $MgCl_2$ (110) surface in the chelate mode are given in Table 3.

Table 3. Adsorption energies (E_{ads}) and O-Mg distances of the five salicylate donors (SID-1–SID-5) and diisobutyl phthalate (DIBP) adsorbed on the pre-activated $MgCl_2$ (110) surface with the preferred chelate mode.

Chelate Mode	E_{ads} (kcal/mol)	Distance (Å)			
		O_1-Mg	O_2-Mg	O_3-Mg	O_4-Mg
SID-1	−37.8	2.04	4.18	2.08	3.64
SID-2	−42.8	2.05	4.18	2.10	3.61
SID-3	−42.0	2.04	4.18	2.09	3.58
SID-4	−51.2	2.03	4.17	2.09	3.58
SID-5	−48.6	2.02	4.17	2.09	3.67
DIBP	−38.7	2.03	3.78	2.07	4.01

Lee et al. [20] found the relationship between adsorption energies of 1,3-diether donors to the $MgCl_2$ surface and the isotacticity and the productivity of polypropylene. Moreover, Ratanasak et al. [56] have studied the relation between the adsorption energies of various classes of electron donors to the catalyst surface and activities. They found that the activity of polypropylene production linearly varies with the adsorption energy. We have made a plot between the experimental PP activity and the adsorption energy (E_{ads}) of the five salicylate donors (SID-1–SID-5), together with that of diisobutyl phthalate (DIBP), as shown in Figure 4.
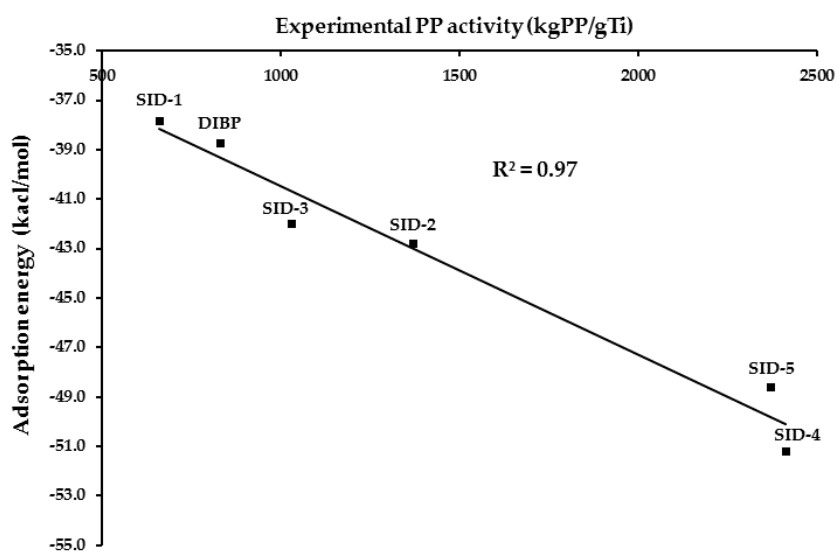

Figure 4. Relationship between the calculated adsorption energy and the experimental polypropylene (PP) activity of five salicylate (SID) and diisobutyl phthalate (DIBP) donors.

From Figure 4, the plot showed the squared correlation coefficient (R^2) of 0.97. This high R^2 value exhibits the linear relation between adsorption energies and PP activities. Hence, our hypothesis on the representative of the adsorption energy of the electron donor to the catalyst surface for the activity of the propylene polymerization is confirmed. Thus, the salicylate donor with the strongest adsorption energy (highest negative value) provides the highest activity for the ZN catalyst. This information is useful for the future design of new electron donors. Moreover, the adsorption energy of diisobutyl phthalate donor is just −38.7 kcal/mol) and three-fourths of our best salicylate donor (SID-4). Thus, DIBP is less active than most of the salicylate donors studied here. We analyzed the dependence of the adsorption energy with the substituent group at R_1, R_2, and R_3 positions for five salicylate donors. The increase of the adsorption energy with the size of R_1 and R_2 substituents was observed. Having the same substituents at R_2 and R_3, while increasing the size of the substituent at R_1 position from H (hydrogen) to Me (methyl), SID-3 has improved E_{ads} of SID-1 by 4.2 kcal/mol. Changing both H at R_1 and R_2 by *i*Pr, (isopropyl) E_{ads} of SID-4 is lowered from SID-1 by 13.4 kcal/mol and when changing by *t*Bu (tertiarybutyl) the adsorption is stronger by 10.8 kcal/mol for SID-5. However, when substituting R_3 of SID-3 by *t*Bu, E_{ads} of SID-2 is enhanced by only 0.8 kcal/mol. Thus, to enhance the catalytic activity of ZN R_3 of the salicylate donor can be either Ph (phenyl) or *t*Bu while R_1 and R_2 should be a bulky group. Our results demonstrated that the size of substituents plays a key role in controlling the adsorption energy. The salicylate donor, which provides strong adsorption energy, should have a bulky group at the R_1 and R_2 positions, and a phenyl or tertiary butyl group at the R_3 position.

3.3. Activation Energies and Stereoselectivities

From Figure 3, the most stable *i*Bu growing chain conformation is 1,2-*re*, A. Thus, the 1,2-*re* propylene insertion on the front side is the preferred pathway for the study of the reactivity and stereoselectivity of five salicylate donors. Considering the 1,2-*si* insertion, the conformation 1,2-*si*, A is the most favorable

route, but it has less stable energy than the 1,2-*re*, A conformation by 3.9 kcal/mol. For the π-complex, we observed that the position of isopropyl substituents on the donors is closer to the methyl moiety of PP in the *re* enantioface than in the *si* enantioface. Thus, the π-complex of the *re* enantioface is probably stabilized by the dispersion-type interaction between the methyl moiety and the substituents.

According to Cossee and Arlman [33–35] and Brookhart and Green [36], the insertion step involves the π-complex formation between the active catalyst and the olefin, the formation of the four-centered transition state, and the generation of the insertion product. Thus, the π-complex formation energy (ΔE_π) and the intrinsic activation energy (E_a) (the energy difference between the transition state structure (TS) and the π-complex) can be used to assess the reactivity of the ZN catalysts. Since the flexible cluster model is employed in this work, the π-complexation energy is then included the relaxation of the surface apart from the coordination energy. The stereoselectivity of polypropylene can be evaluated from the relative barrier (Rel.), which is the difference between the TS energy of 1,2-*si* ($E_{TS}(si)$) and 1,2-*re* ($E_{TS}(re)$) insertions. Additionally, it is also useful to estimate the apparent activation energy ($E_a(app)$) which is $\Delta E_\pi + E_a$ and equivalent to the transition state energy relative to the dissociation channel of the catalyzed PP polymerization. Since the chelate mode was the preferred adsorption mode for salicylate donors, this mode was then selected for the construction of the active $MgCl_2$ (110) surface. Table 4 lists π-complex formation energy, intrinsic activation energy, apparent activation energy, and relative barrier for the insertion step of the ZN-catalyzed PP polymerization with five salicylate donors.

Table 4. The π-complex formation energy (ΔE_π), the intrinsic activation energy (E_a), the relative barrier (Rel.), and the apparent activation energy ($E_a(app)$) of the ZN-catalyzed PP polymerization with the five salicylate donors together with values of transition state imaginary frequencies (ν).

SID	Insertion	ΔE_π (kcal/mol)	E_a (kcal/mol)	$E_a(app)$ (kcal/mol)	Rel. (kcal/mol)	ν (cm^{-1})
1	1,2-*si*	−59.5	6.4	−53.1	1.1	−340*i*
	1,2-*re*	−63.1	9.0	−54.1		−339*i*
2	1,2-*si*	−58.0	5.1	−52.9	3.5	−344*i*
	1,2-*re*	−62.6	6.1	−56.5		−354*i*
3	1,2-*si*	−58.1	5.7	−52.4	3.2	−331*i*
	1,2-*re*	−63.5	7.9	−55.6		−345*i*
4	1,2-*si*	−59.2	3.9	−55.3	3.9	−332*i*
	1,2-*re*	−63.2	4.6	−58.6		−340*i*
5	1,2-*si*	−58.8	4.4	−54.5	3.6	−362*i*
	1,2-*re*	−62.7	4.8	−57.9		−375*i*

The π-complex formation energies (ΔE_π) of the five salicylate donors are in the range of −58—64 kcal/mol. Generally, the 1,2-*re* insertion complex gives lower ΔE_π than its 1,2-*si* counterpart, suggesting the more stable π-complex of the 1,2-*re* insertion mode. Structures of the π-complex of (a) 1,2-*re* and (b) 1,2-*si* insertions of ZN-catalyzed PP polymerization with the salicylate (SID-4) donor are shown in Figure 5. From Figure 5, we observed that the position of isopropyl substituents on the donors is closer to the methyl moiety of PP in the *re* enantioface π-complex than in the *si* enantioface. Thus, the *re* enantioface π-complex is probably stabilized by the dispersion-type interaction between the methyl moiety and the substituents. The π-complex of 1,2-*re* insertion for the case of SID-3 provides the strongest ΔE_π (−63.5 kcal/mol), while that of 1,2-*si* for SID-2 gives the weakest interaction (−58.0 kcal/mol). There seems to be no direct relationship between activity and ΔE_π. Comparing with DIBP (−37.4 kcal/mol for 1,2-*si* and −41.7 kcal/mol for 1,2-*re* insertions [23]), π-complex formation energies of all primary(1,2) insertion modes for five salicylates are larger. However, the π-complexation energy of the ZN without the electron donor is only −30 (*si* face) and −33 (*re* face) kcal/mol [17], which suggests that the electron donor stabilizes the π-complex.
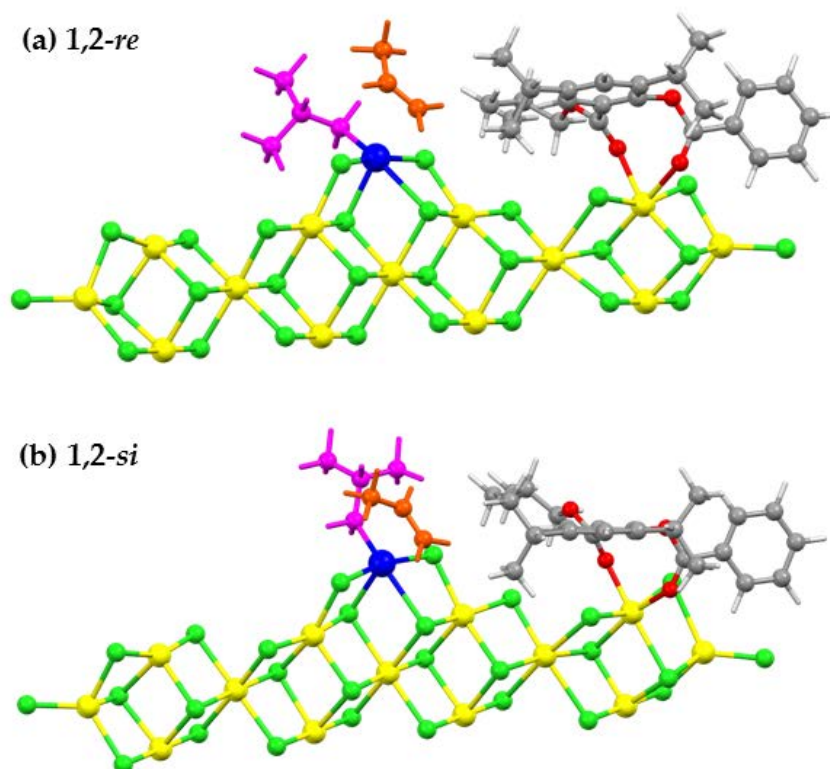
Figure 5. Structures of the π-complex of (**a**) 1,2-*re* and (**b**) 1,2-*si* insertions of the ZN-catalyzed PP polymerization with the salicylate (SID-4) donor.

Intrinsic activation energies (E_a) of the five salicylate donors for both insertion modes are between 3.9 to 9.0 kcal/mol, and the 1,2-*re* insertion has a higher activation barrier than its corresponding 1,2-*si*. This similar trend was also found for the 1,2-*re* /1,2-*si* insertion with DIBP (4.7/4.5 kcal/mol) and dibenzoyl sulfide (6.5/4.4 kcal/mol) [23]. When we considered the relationship between the intrinsic activation energies of 1,2-*re* and 1,2-*si* insertions and the log of experimental PP activities of five salicylate donors, we found $R^2 = 0.98$ and 0.97, respectively. Thus, the ln(activity) is directly related to the intrinsic activation barrier of the insertion step. (For the first-order kinetics, ln$k = -E_a/RT$). The lowering of the activation barrier will enhance the activity of the ZN catalyst. There seems to be a relation between $E_a(app)$ and the ln(activity). We obtained R^2 of 0.99 and 0.64 for the $E_a(app)$ of the 1,2-*re* and -*si* insertions, respectively. The activity is related to the TS energy of the 1,2-*re* insertion. Thus, the donor which can better stabilize TS energy of 1,2-*re* insertion will provide a higher activity for the catalyst. Interestingly, while ΔE_π does not have any relation to the activity, the E_a and $E_a(app)$ do. We also found a correlation between $E_a/E_a(app)$ and E_{ads} to be around 0.94. This suggests that factors which provide high adsorption energy will be the same for $E_a/E_a(app)$.

Moreover, we found the highest occupied molecular orbital (HOMO) energies of SID-1 to SID-5 donors (-0.249, -0.242, -0.247, -0.238 and -0.235 a.u., respectively) to be also linearly related to ln(PP activity) with $R^2 = 0.94$. The donor with higher HOMO provides higher activity for the ZN catalyst. More interestingly, with the least square fit for E_a of 1,2-*re* and 1,2-*si* insertions and HOMO we obtained R^2 of 0.94 and 0.87, respectively. Thus, HOMO data is better correlated with E_a of 1,2-*re* insertion. The relation between HOMO and E_a could be well explained by the Frontier Molecular Orbitals (FMO). This information suggests that the more potent salicylate donors should have high HOMO energy (less negative value). However, we should restrict our observation to within the same class of compounds.

Figure 6 illustrates the transition state structures of two enantiofaces of the primary (1,2) insertion modes of the ZN-catalyzed PP polymerization with SID-4. From the Figure, it appears that TS structures are similar to the corresponding π-complex structures, where the methyl moiety of PP is positioned

furthest from the donor in the primary (1,2)-*si*, and in the primary (1,2)-*re* they are in the close vicinity. If the E_a for the insertion step is controlled solely by the steric interaction between the methyl moiety of PP and the substituents of the donor, as suggested by Cavallo et al. [39], the TS of the 1,2-*re* insertion should be less stable (higher) than that of the 1,2-*si*. From the values of E_a(app) in Table 4, the energy of the TS of the 1,2-*re* insertion is lower than that of 1,2-*si* for all electron donors. In other words, the TS of the 1,2-*re* with salicylate donor is more stable than the TS of the 1,2-*si*. Thus, the close encounter of the methyl moiety of PP and substituents on the donor provides a favorable interaction to the TS of 1,2-*re* insertion. Thus, the dispersion-type interaction should be another effect. To prove our hypothesis, the π-complex formation energy (ΔE_{π}), the intrinsic activation energy (E_a), the relative barrier (Rel.), and the apparent activation energy (E_a(app)) of the five salicylate donors (SID-1–5) were calculated using the B3LYP method. These values are given in Table S3 in supporting information. The values in Table S3 differ from those in Table 4. This suggests the importance of dispersion interaction. However, without dispersion (values in Table S3) the (1,2)-*re* remains the preferred insertion mode for salicylate donors (noticing from E_a(app), and Rel.), in exception of SID-1. Thus, we still believed that the stereoselectivity of the ZN catalyst is controlled by the steric interaction between the electron donor and the methyl moiety of propylene, in agreement with Corradini [52], Cavallo [39], and the Taniike groups [26]. However, the (1,2)-*re* insertion gains extra stability from the dispersion interaction. Unlike when the B3LYP-D3 method was employed for the calculations, no relation between computed values of ΔE_{π} or E_a or Rel. or E_a(app)) and the activities of the five salicylate donors was observed when the calculations were performed using B3LYP (see Table S4). This implies the significance of the dispersion-type interaction for this system. Therefore, we can conclude that there exists a dispersion-type interaction between the methyl moiety of PP and the substituents of the donors, which helps to stabilize the TS of the 1,2-*re* insertion. The higher activation energy of the 1,2-*re* insertion mainly comes from the stronger π-complex formation of the *re* enantioface.

The polymerization can be determined by relative barriers (Rel.). Theoretically, higher Rel. would relate to the higher stereoselectivity. The relative barrier of ZN-catalyzed PP polymerization with the five salicylate donors of SID-1 to SID-5 are given in Table 4. Experimentally, the stereoselectivity can be indicated by the percent isotactic sequence length (%mm) and isotacticity index (%I.I). These values for the five salicylate donors are listed in Table 1. The positive value of the relative barrier indicates that the TS with a *re*-coordinated propylene face is more stable than the corresponding *si*-enantioface. From the result, the SID-4 system gave the highest value for the relative barrier (3.9 kcal/mol) and hence the highest stereoselectivity (%mm = 91.0 and %I.I = 98.6). The SID-1 system has the lowest relative barrier (1.1 kcal/mol) and the lowest selectivity (%mm = 85.5 and %I.I = 96.3). Compared with the industrial diisobutyl phthalate donor, we have previously reported that the transition state for the primary (1,2)-*re* is 4.0 kcal/mol below that for primary (1,2)-*si*. [23]. The %mm and %I.I of PP prepared by the diisobutyl phthalate internal donor are 91.0% and 91.7%, respectively [16]. Thus, the relative barrier of the ZN-catalyzed PP polymerization correlates well with the experimental stereospecificity data [16]. Also, the %selectivity, which should be closely related to both %mm and %I.I., can be estimated using the Curtin-Hammett principle (see the details in Table S6 of Supporting Information). The linear relationship between the %selectivity for the five salicylate donors and %mm and %I.I was observed with R^2 of 0.74 and 0.55, respectively. Since the substituents on the electron donor play roles in the stability of the TS of the 1,2-*re* insertion as mentioned earlier, types of substituents on the donor can be used to assess the selectivity of the ZN catalyst. The SID-1 donor which has the lowest Rel. (1.0 kcal/mol) contains an H atom as the substituent for R_1 and R_2 and phenyl for R_3. The SID-4 donor with *i*Pr on R_1 and R_2 while having the same substituent on R_3 as the SID-1 gives the largest Rel. (3.9 kcal/mol). Similarly, with *t*Bu on R_2 and R_3, the SID-5 also has large Rel. (3.6 kcal/mol). Thus, the substituents on R_1 and R_2 enhance the stability of the TS for 1,2-*re* insertion towards that for 1,2-*si*. The *i*Pr substituent provides a more favorable interaction than *t*Bu. Possibly the *t*Bu is too bulky. The R_3 substituent plays a smaller role than those on R_1 and R_2, since it gives a small difference for the relative barriers of SID-2 (3.5 kcal/mol) and SID-3 (3.2 kcal/mol). It should be noted that suggestions for

improving stereoselectivity by salicylate electron donors are the same as those for improving activity. Therefore, the salicylate donor that provides high activity will also provide high stereoselectivity.
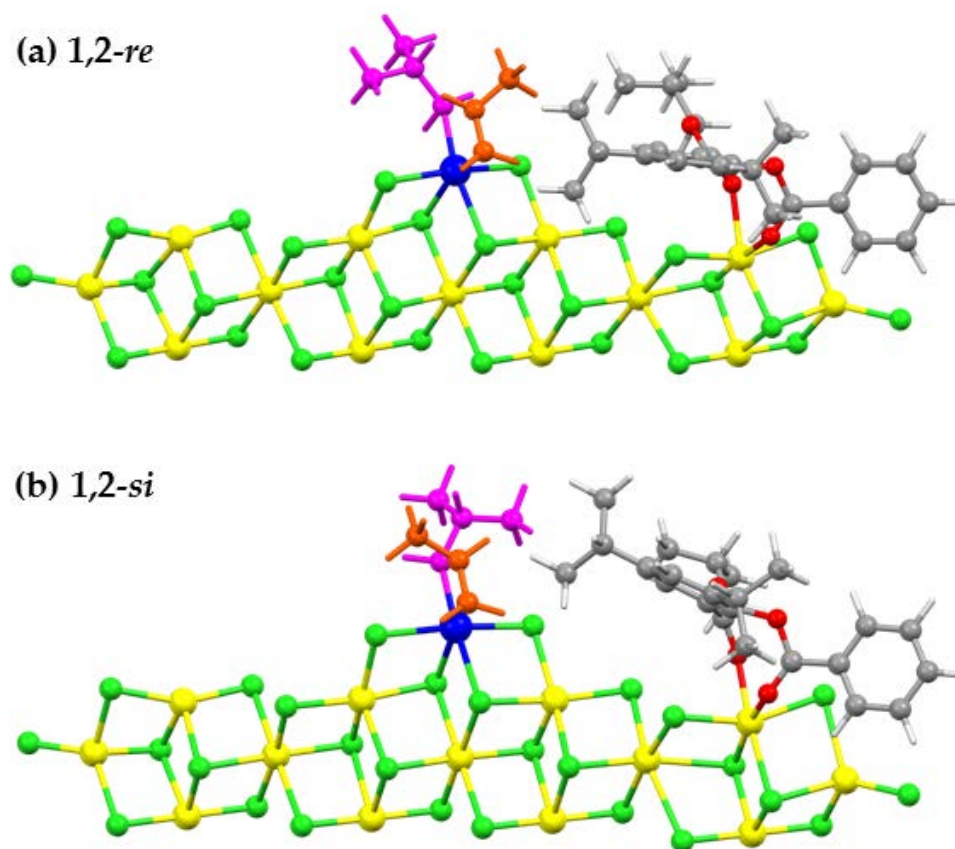

Figure 6. Structures of the transition sates of (**a**) 1,2-*re* and (**b**) 1,2-*si* insertions of ZN-catalyzed PP polymerization with salicylate (SID-4) donor.

3.4. Comparing with Other Internal Electron Donors

The isobutyl 2-benzyloxy-3,5-isopropyl benzoate or salicylate donor (SID-4) was selected to represent five salicylate donors, since this compound gives the highest activity [16]. Apparent activation energies (E_a(app)) of primary (1,2)-*re* insertion in kcal/mol, relative barrier (Rel.) in kcal/mol, activity in kg-PP/gCat for di-*n*-butyl-2-cyclopentyl malonate, dibenzoyl sulfide, diisobutyl phthalate donors and in kg-PP/gTi for diisobutyl phthalate and salicylate donors, and %isotacticity in %mmmm (pentrad) for di-*n*-butyl-2-cyclopentyl malonate, dibenzoyl sulfide, diisobutyl phthalate donors, and in %mm (triad) for diisobutyl phthalate and salicylate donors are listed in Table 5. In our previous work, we have shown that E_a(app) can be used on par with the experimental activity [23]. Thus, it was used for the comparison of the activity of the ZN catalyst with various electron donors, whereas Rel. was utilized for comparing %isotacticity.

Among all internal electron donors in Table 5, the ZN catalyst with salicylate donor (SID-4) gives the lowest (highest negative) E_a(app) and hence, the best activity. This is followed by those with dibenzoyl sulfide, di-*n*-butyl-2-cyclopentyl malonate, and diisobutyl phthalate donors, which have a higher E_a(app) (less negative) and, thus, less activity. The apparent activation energy of the ZN catalyst without a donor is the least negative and, therefore, the catalyst shows the poorest activity. In the order of experimental activity, the list of donors is sulfide > malonate, phthalate. This order agrees with the calculated apparent activation energies. Unfortunately, the salicylate donor (SID-4) does not share the same unit for activity. Thus, it cannot be directly compared with other internal donors. By comparing E_a(app), the ZN catalyst with the salicylate donor probably yields similar activity to that of sulfide

donor. Using data of malonate, sulfide, and phthalate donors, we obtained a linear equation between ln(activity) and E_a(app) with R^2 of 0.98. From the equation, we estimated the activity of the ZN catalyst with salicylate donor to be 40.4 kg-PP/gCat.

Table 5. Apparent activation energy (E_a(app)) of primary (1,2)-*re* insertion, relative barrier (Rel.), experimental activity, and %isotacticity of ZN-catalyzed PP polymerization in absence of donor (*w/o* donor) and with malonate, sulfide, phthalate, and salicylate donors.

1,2-*re* Insertion	Theoretical Predictions			Experiments		
	E_a(app) (kcal/mol)	Rel. (kcal/mol)	Ref.	Activity (kg-PP/gCat)	%Isotacticity (%mmmm)	Ref.
w/o donor	−26.6	0.2	[17]	-	-	
Malonate [i]	−38.5 [ac]	−1.5	[17]	25	97.5	[13]
Sulfide [ii]	−58.2	11.9	[23]	40	91.7	[57]
Phthalate [iii]	−37.0	4.0	[23]	22	88.7	[57]
				830 [b]	91.7 [c]	[16]
Salicylate [iv]	−58.6	3.9		2410 [b]	91.0 [c]	[16]

[i] Di-*n*-butyl-2-cyclopentyl malonate; [ii] Dibenzoyl sulfide; [iii] Diisobutyl phthalate; [iv] Isobutyl 2-benzyloxy-3,5-isopropyl benzoate (SID-4); [a] primary(1,2)-*si* insertion; [b] Activity in (kg-PP/gTi); [c] %Isotacticity in %mm.

Excluding data of the malonate donor in Table 5, it can be seen that the %Isotacticity is well predicted by the relative barrier (Rel.) [16]. The ZN with sulfide donor gives Rel. of 11.9 kcal/mol and has a %mmmm of 91.7, while that with phthalate donor gives Rel. of 4.0 kcal/mol and have %mmmm of 88.7 [23]. The salicylate donor which has comparable Rel. to the phthalate donor provides the polypropylene product with similar %isotacticity. Interestingly, the malonate donor has a negative relative barrier, implying that the TS for the 1,2-*si* insertion is more stable. Moreover, the ZN catalyst with the malonate donor yields the polypropylene product with better %isotacticity (%mmmm = 97.5) than that with the sulfide donor [13]. Thus, the interaction involved in the insertion step of the ZN-catalyzed PP polymerization with the malonate donor must be different from others.

The relative barrier can be decomposed to contributions from ΔE_π and E_a. Since the transition state energy relative to the dissociation channel (E_{TS}) is E_a(app) and Rel. $= E_{TS}(si) - E_{TS}(re)$. Therefore,

$$\text{Rel.} = \Delta\Delta E_\pi + \Delta E_a$$

where $\Delta\Delta E_\pi = \Delta E_\pi(si) - \Delta E_\pi(re)$, and $\Delta E_a = E_a(si) - E_a(re)$. The decomposition of the relative barrier of malonate, sulfide, phthalate, and salicylate (SID-4) donors is given in Table 6.

Table 6. Differences between *re* and *si* enantiofaces of π-complexation energies ($\Delta\Delta E_\pi$), intrinsic activation energies (ΔE_a), and transition state energies of the primary (1,2) insertion step (relative barrier, Rel.).

Electron Donor	$\Delta\Delta E_\pi$ (kcal/mol)	ΔE_a (kcal/mol)	Rel. (kcal/mol)
Malonate	1.6	−3.1	−1.5
Sulfide	14.0	−2.1	11.9
Phthalate	4.3	−0.3	4.0
Salicylate	3.9	−0.7	3.9

The positive sign of the value means that the value for the *re* face of the propylene monomer is lower than that of the *si* face and vice versa. From Table 6, the contribution of ΔE_π to the relative barrier favors the *re* face insertion, while that of E_a favors the *si* face insertion for all donors. Thus, the nature of interactions that controlled the stereoselectivity is the same for all donors. However, for salicylate, sulfide, and phthalate donors, the magnitude of the ΔE_π contribution is larger than that of the E_a contribution. Thus, the selectivity is dictated by the contribution of ΔE_π and *re* face insertion

is preferred. Whereas it is contrary to the malonate donor. Therefore, the selectivity is controlled by the E_a contribution and the *si* face insertion is preferred.

4. Conclusions

The preferred adsorption mode of salicylate donors is the chelate mode, similar to malonate [17], dibenzoyl sulfide [23], and diisobutyl phthalate [23] donors. The carbonyl O-Mg coordinated distances for the chelate mode are between 2.02–2.10 Å. A good linear relation between adsorption energies of the five salicylate donors and the experimental PP activity was noticed with $R^2 = 0.96$, implying that salicylate donors with the strongest adsorption energy will provide the ZN catalyst with the highest activity. This finding is in line with our previous work on other donors [23]. Salicylate donors (SID-2 to SID-5) have lower adsorption energies (−42.8 to −51.2 kcal/mol) than that of the diisobutyl phthalate (DIBP) donor (−38.7 kcal/mol). Our results also demonstrated that the size of substituents plays a key role in controlling the adsorption energy. The salicylate donor which provides strong adsorption energy should have a bulky group at the R_1 and R_2 positions and a phenyl or tertiary butyl group at the R_3 position.

The insertion step which is the RDS for olefin polymerization involves the π-complex formation and the activation of olefin insertion. Thus, the activity of PP polymerization can be estimated from the π-complex formation energy (ΔE_π) and the intrinsic activation energy (E_a). The ΔE_π for the five salicylate donors were reported to be between −58.0–−59.5 kcal/mol and −62.6–−63.5 kcal/mol for the *si* and the *re* enantioface complexes, respectively. Most salicylate donors have a stronger π-complexation energy than DIBP. The intrinsic activation energy for 1,2-*si* and -*re* insertions of the ZN with the five salicylate donors are 3.9–6.4 and 4.6–9.0 kcal/mol, respectively. The corresponding apparent activation energies in the respective order of 1,2-*si* and 1,2-*re* insertions are −53.1–−55.3 and −54.1–−58.6 kcal/mol. No relation between ΔE_π and activity was observed. However, we found the linear relation between the intrinsic activation energy and the ln(experimental activity) with R^2 of 0.98 and 0.97 for the primary(1,2)-*re* and (1,2)-*si* insertion, respectively. The apparent activation energy (E_a(app)) which is $\Delta E_\pi + E_a$ and equivalent to the transition state (TS) energy in relative to the dissociation channel of five donors has the R^2 with the ln(activity) of 0.99 and 0.64 for the 1,2-*re* and (1,2)-*si*, respectively. Thus, the activity also strongly correlates with E_a(app) for 1,2-*re* insertion. For E_a and E_a(app), the lowering of the value causes an increase in the activity of the ZN catalyst. The highest occupied molecular orbital (HOMO) energy of the salicylate donor was as well found to show the strong correlation with both the ln(activity) ($R^2 = 0.94$) and E_a of 1,2-*re* insertion ($R^2 = 0.94$). The relation between HOMO and E_a could be explained by the frontier molecular orbital. Moreover, the relation between E_a/E_a(app) and adsorption energies was observed ($R^2 = 0.94$). Thus, electron donors which have strong adsorption to the catalyst also provide low E_a/E_a(app) for the insertion step of PP polymerization.

The stereoselectivity can be estimated from the relative stability between TS structures of 1,2-*si* and -*re* insertions or the relative barrier (Rel.). For the five salicylate donors, the transition state of the 1,2-*re* insertion has lower energy than that of the 1,2-*si* insertion. Thus, the salicylate donors provide stereoselectivity for the ZN catalyst. Relative barriers of the five salicylate donors are 1.0 (SID-1) to 3.9 (SID-4) kcal/mol. Thus, SID-4 provides the best stereoselectivity for this series. Furthermore, Rel. can be used to predict %Isotacticity. It provides R^2 of 0.79 and 0.61 with the percent isotactic sequence length (%mm) and isotacticity index (%I.I), respectively. Relative barriers for SID-4 and DIBP are 3.9 and 4.0 kcal/mol, respectively, is following the experimental %mm of 91.0 and 91.7%. Therefore, the salicylate donor with the largest relative barrier will give the highest stereoselectivity. We found similar substituent effects in controlling activity and stereoselectivity. The electron donor which can yield high productivity will also give high stereoselectivity.

The apparent activation energy and the relative barrier can also be used to predict the activity and stereoselectivity of other electron donors. The order of donors according to the activity is isobutyl 2-benzyloxy-3,5-isopropyl benzoate (SID-4) > dibenzoyl sulfide (sulfide) > di-*n*-butyl-2-cyclopentyl malonate (malonate) > diisobutyl phthalate (phthalate). For the selectivity (excluding malonate),

the order is sulfide > phthalate > salicylate. The relative barrier can be decomposed to contributions from τηε π-complex formation ($\Delta\Delta E_\pi$) and insertion activation energy (ΔE_a). The $\Delta\Delta E_\pi$ prefers *re* enantioface while the ΔE_a prefers *si* enantioface. For most donors, the magnitude of $\Delta\Delta E_\pi$ is larger than ΔE_a. Therefore, 1,2-*re* insertion is favored. For the malonate donor, ΔE_a is larger and the 1,2-*si* insertion is preferred.

Supplementary Materials: The following are available online at http://www.mdpi.com/2073-4360/12/4/883/s1, Figure S1: Chelate adsorption modes of five salicylate donors (SID-1−SID-5) and diisobutyl phthalate (DIBP) donor on the ZN catalyst, Table S1: NBO charges on the O_1-O_4 oxygen of five salicylate donors (SID-1−SID-5) and diisobutyl phthalate (DIBP) donor, Table S2: Adsorption energies (E_{ads}) of five salicylate donors (SID) with different substituent groups at R_1, R_2 and R_3 positions and experimental data [16] adsorbed on the pre-activated $MgCl_2$(110) surface with the preferred chelate mode using B3LYP-D3 and B3LYP, Table S3: The π-complex formation energy (ΔE_π), the intrinsic activation energy (E_a), the relative barrier (Rel.), and the apparent activation energy (E_a(app)) of the ZN catalyzed PP polymerization with five salicylate donors together using B3LYP calculations, Table S4: The correlation between calculated parameters (E_{ads}, E_a, ΔE_π $E_{a(app)}$, and Rel.) using the B3LYP-D3 calculations and experimental results (Activity, %mm and %I.I.) of five salicylate donors (SID) from reference [16], Table S5: The correlation between calculated parameters (E_{ads}, E_a, ΔE_π $E_{a(app)}$, and Rel.) using the B3LYP calculations and experimental results (Activity, %mm and %I.I.) of five salicylate donors (SID) from reference [16]., Table S6: Five salicylate donors (SID) and %mm and %I.I. from the experimental results [16] and the relative barrier (Rel.) from B3LYP-D3 calculations and % selectivity from eq. 1 at temperature 343 K.

References

1.　Yao, Z.-J.; Deng, W. Half-sandwich late transition metal complexes based on functionalized carborane ligands. *Coord. Chem. Rev.* **2016**, *309*, 21–35. [CrossRef]

2.　Shamiri, A.; Chakrabarti, M.; Jahan, S.; Hussain, M.; Kaminsky, W.; Aravind, P.; Yehye, W. The Influence of Ziegler-Natta and Metallocene Catalysts on Polyolefin Structure, Properties, and Processing Ability. *Materials* **2014**, *7*, 5069–5108. [CrossRef]

3.　Maddah, H.A. Polypropylene as a Promising Plastic: A Review. *Am. J. Polym. Sci.* **2016**, *6*, 1–11.

4.　Shumilo, O.N.; Bulgakov, N.N.; Likholobov, V.A. On the mechanism of ethylene and propylene insertion into metal-hydroxo bonds. *Reacti. Kineti. Catal. Lett* **1983**, *22*, 87–93. [CrossRef]

5.　Sacchi, M.C.; Tritto, I.; Shan, C.; Mendichi, R.; Noristi, L. Role of the pair of internal and external donors in magnesium chloride-supported Ziegler-Natta catalysts. *Macromolecules* **1991**, *24*, 6823–6826. [CrossRef]

6.　Soga, K.; Shiono, T.; Doi, Y. Influence of internal and external donors on activity and stereospecificity of ziegler-natta catalysts. *Makromol. Chem.* **1988**, *189*, 1531–1541. [CrossRef]

7.　Ferreira, M.a.L.; Damiani, D.E. Effect of different donors on kinetics of Zn catalysts and molecular weight of the obtained polypropylene. *J. Mol. Catal. Chem.* **1999**, *150*, 53–69. [CrossRef]

8.　Morini, G.; Albizzati, E.; Balbontin, G.; Mingozzi, I.; Sacchi, M.C.; Forlini, F.; Tritto, I. Microstructure Distribution of Polypropylenes Obtained in the Presence of Traditional Phthalate/Silane and Novel Diether Donors: A Tool for Understanding the Role of Electron Donors in MgCl2-Supported Ziegler−Natta Catalysts. *Macromolecules* **1996**, *29*, 5770–5776. [CrossRef]

9.　Singh, G.; Kaur, S.; Makwana, U.; Patankar, R.B.; Gupta, V.K. Influence of Internal Donors on the Performance and Structure of MgCl2 Supported Titanium Catalysts for Propylene Polymerization. *Macromol. Chem. Phys.* **2009**, *210*, 69–76. [CrossRef]

10.　Guo, J.; Hu, G.; Chen, Z. Synthesis of novel electron donors and their application to propylene polymerization. *Trans. Tianjin Univ.* **2012**, *18*, 8–14. [CrossRef]

11. Cui, N.; Ke, Y.; Li, H.; Zhang, Z.; Guo, C.; Lv, Z.; Hu, Y. Effect of diether as internal donor on MgCl2-supported Ziegler–Natta catalyst for propylene polymerization. *J. Appl. Polym. Sci* **2006**, *99*, 1399–1404. [CrossRef]

12. Brambilla, L.; Zerbi, G.; Piemontesi, F.; Nascetti, S.; Morini, G. Structure of Donor Molecule 9,9-Bis (Methoxymethyl)-Fluorene in Ziegler-Natta Catalyst by Infrared Spectroscopy and Quantum Chemical Calculation. *J. Phys. Chem. C* **2010**, *114*, 11475–11484. [CrossRef]

13. Tanase, S.; Katayama, K.; Yabunouchi, N.; Sadashima, T.; Tomotsu, N.; Ishihara, N. Design of novel malonates as internal donors for MgCl2-supported TiCl4 type polypropylene catalysts and their mechanistic aspects, Part 1. *J. Mol. Catal. A* **2007**, *273*, 211–217. [CrossRef]

14. Liu, B.; Cheng, R.; Liu, Z.; Qiu, P.; Zhang, S.; Taniike, T.; Terano, M.; Tashino, K.; Fujita, T. Experimental and Computational Approaches on the Isospecific Role of Monoester-Type Internal Electron Donor for TiCl4/MgCl2 Ziegler-Natta Catalysts. *Macromol. Symp.* **2007**, *260*, 42–48. [CrossRef]

15. Marques, M.d.F.V.; Cardoso, R.d.S.; da Silva, M.G. Preparation of MgCl2-supported Ziegler–Natta catalyst systems with new electron donors. *Appl. Catal. A* **2010**, *374*, 65–70. [CrossRef]

16. Zhou, Q.; Wang, A.; Li, H.; Luo, Z.; Zheng, T.; Zhang, L.; Hu, Y. Microstructure of polypropylene and active center in Ziegler-Natta catalyst: Effect of novel salicylate internal donor. *RSC Adv.* **2016**, *6*, 75023–75031. [CrossRef]

17. Ratanasak, M.; Parasuk, V. Roles of malonate donor on activity and stereoselectivity of Ziegler–Natta catalyzed propylene polymerization. *J. Organomet. Chem.* **2015**, *775*, 6–11. [CrossRef]

18. Cavallo, L.; Del Piero, S.; Ducéré, J.-M.; Fedele, R.; Melchior, A.; Morini, G.; Piemontesi, F.; Tolazzi, M. Key Interactions in Heterogeneous Ziegler−Natta Catalytic Systems: Structure and Energetics of TiCl4−Lewis Base Complexes. *J. Phys. Chem. C* **2007**, *111*, 4412–4419. [CrossRef]

19. Correa, A.; Credendino, R.; Pater, J.T.M.; Morini, G.; Cavallo, L. Theoretical Investigation of Active Sites at the Corners of MgCl2 Crystallites in Supported Ziegler–Natta Catalysts. *Macromolecules* **2012**, *45*, 3695–3701. [CrossRef]

20. Lee, J.W.; Jo, W.H. Chemical structure–stereospecificity relationship of internal donor in heterogeneous Ziegler–Natta catalyst for propylene polymerization by DFT and MM calculations. *J. Organomet. Chem.* **2009**, *694*, 3076–3083. [CrossRef]

21. Toto, M.; Morini, G.; Guerra, G.; Corradini, P.; Cavallo, L. Influence of 1,3-Diethers on the Stereospecificity of Propene Polymerization by Supported Ziegler−Natta Catalysts. A Theoretical Investigation on Their Adsorption on (110) and (100) Lateral Cuts of MgCl2 Platelets. *Macromolecules* **2000**, *33*, 1134–1140. [CrossRef]

22. Vanka, K.; Singh, G.; Iyer, D.; Gupta, V.K. DFT Study of Lewis Base Interactions with the MgCl2 Surface in the Ziegler−Natta Catalytic System: Expanding the Role of the Donors. *J. Phys. Chem. C* **2010**, *114*, 15771–15781. [CrossRef]

23. Ratanasak, M.; Parasuk, V. Understanding the roles of novel electron donors in Ziegler-Natta catalyzed propylene polymerization. *RSC Adv.* **2016**, *6*, 112776–112783. [CrossRef]

24. Mukhopadhyay, S.; Kulkarni, S.A.; Bhaduri, S. Density functional study on the role of electron donors in propylene polymerization using Ziegler–Natta catalyst. *J. Organomet. Chem.* **2005**, *690*, 1356–1365. [CrossRef]

25. Taniike, T.; Terano, M. Coadsorption and Support-Mediated Interaction of Ti Species with Ethyl Benzoate in MgCl2-Supported Heterogeneous Ziegler-Natta Catalysts Studied by Density Functional Calculations. *Macromol. Rapid Commun.* **2007**, *28*, 1918–1922. [CrossRef]

26. Taniike, T.; Terano, M. Coadsorption model for first-principle description of roles of donors in heterogeneous Ziegler–Natta propylene polymerization. *J. Catal.* **2012**, *293*, 39–50. [CrossRef]

27. Shen, X.-R.; Fu, Z.-S.; Hu, J.; Wang, Q.; Fan, Z.-Q. Mechanism of Propylene Polymerization with MgCl2-Supported Ziegler–Natta Catalysts Based on Counting of Active Centers: The Role of External Electron Donor. *J. Phys. Chem. C* **2013**, *117*, 15174–15182. [CrossRef]

28. Wondimagegn, T.; Ziegler, T. The Role of External Alkoxysilane Donors on Stereoselectivity and Molecular Weight in MgCl2-Supported Ziegler–Natta Propylene Polymerization: A Density Functional Theory Study. *J. Phys. Chem. C* **2012**, *116*, 1027–1033. [CrossRef]

29. Credendino, R.; Pater, J.T.M.; Liguori, D.; Morini, G.; Cavallo, L. Investigating Alkoxysilane Coverage and Dynamics on the (104) and (110) Surfaces of MgCl2-Supported Ziegler–Natta Catalysts. *J. Phys. Chem. C* **2012**, *116*, 22980–22986. [CrossRef]

30. Busico, V.; Cipullo, R.; Pellecchia, R.; Ronca, S.; Roviello, G.; Talarico, G. Design of stereoselective Ziegler–Natta propene polymerization catalysts. *Proc. Natl. Acad. Sci. USA* **2006**, *103*, 15321–15326. [CrossRef]

31. Sakai, S. Ab initio studies on the Ziegler–Natta polymerization mechanisms of ethylene and propylene. Role of cocatalysis and stereoregulation. *Int. J. Quantum Chem.* **1997**, *65*, 739–747. [CrossRef]

32. Seth, M.; Ziegler, T. Theoretical Study of the Copolymerization of Ethylene and Propylene by a Heterogeneous Ziegler−Natta Catalyst. *Macromolecules* **2004**, *37*, 9191–9200. [CrossRef]

33. Cossee, P. Ziegler-Natta catalysis I. Mechanism of polymerization of α-olefins with Ziegler-Natta catalysts. *J. Catal.* **1964**, *3*, 80–88. [CrossRef]

34. Arlman, E.J. Ziegler-Natta catalysis II. Surface structure of layer-lattice transition metal chlorides. *J. Catal.* **1964**, *3*, 89–98. [CrossRef]

35. Arlman, E.J.; Cossee, P. Ziegler-Natta catalysis III. Stereospecific polymerization of propene with the catalyst system TiCl3 AlEt3. *J. Catal.* **1964**, *3*, 99–104. [CrossRef]

36. Brookhart, M.; Green, M.L.H. Carbon-hydrogen-transition metal bonds. *J. Organomet. Chem.* **1983**, *250*, 395–408. [CrossRef]

37. Doi, Y.; Suzuki, S.; Nozawa, F.; Soga, K.; Keii, T. Structure and Reactivity of "Living" Polypropylene. In *Studies in Surface Science and Catalysis*; Keii, T., Soga, K., Eds.; Elsevier: Amsterdam, The Netherlands, 1986; Volume 25, pp. 257–270.

38. Brintzinger, H.H.; Fischer, D.; Mülhaupt, R.; Rieger, B.; Waymouth, R.M. Stereospecific Olefin Polymerization with Chiral Metallocene Catalysts. *Angew. Chem. Int. Ed. Engl.* **1995**, *34*, 1143–1170. [CrossRef]

39. Correa, A.; Piemontesi, F.; Morini, G.; Cavallo, L. Key Elements in the Structure and Function Relationship of the MgCl2/TiCl4/Lewis Base Ziegler−Natta Catalytic System. *Macromolecules* **2007**, *40*, 9181–9189. [CrossRef]

40. Xie, K.; Zhu, B.; Xu, R.; Xu, J.; Liu, P. Periodic DFT study of the donor interactions with the MgCl2 surface in the Ziegler-Natta catalytic system. *RSC Adv.* **2016**, *6*, 13137–13144. [CrossRef]

41. Shetty, S. Synergistic, reconstruction and bonding effects during the adsorption of internal electron donors and TiCl4 on MgCl2 surface: A periodic-DFT investigation. *Surf. Sci.* **2016**, *653*, 55–65. [CrossRef]

42. Stukalov, D.V.; Zakharov, V.A.; Zilberberg, I.L. Adsorption Species of Ethyl Benzoate in MgCl2-Supported Ziegler−Natta Catalysts. A Density Functional Theory Study. *J. Phys. Chem. C* **2010**, *114*, 429–435. [CrossRef]

43. D'Amore, M.; Credendino, R.; Budzelaar, P.H.M.; Causá, M.; Busico, V. A periodic hybrid DFT approach (including dispersion) to MgCl2-supported Ziegler–Natta catalysts—1: TiCl4 adsorption on MgCl2 crystal surfaces. *J. Catal.* **2012**, *286*, 103–110. [CrossRef]

44. Andoni, A.; Chadwick, J.C.; Niemantsverdriet, H.J.W.; Thüne, P.C. The role of electron donors on lateral surfaces of MgCl2-supported Ziegler–Natta catalysts: Observation by AFM and SEM. *J. Catal.* **2008**, *257*, 81–86. [CrossRef]

45. Brambilla, L.; Zerbi, G.; Piemontesi, F.; Nascetti, S.; Morini, G. Structure of MgCl2–TiCl4 complex in co-milled Ziegler–Natta catalyst precursors with different TiCl4 content: Experimental and theoretical vibrational spectra. *J. Mol. Catal. A* **2007**, *263*, 103–111. [CrossRef]

46. Grimme, S. Density functional theory with London dispersion corrections. *Wiley Interdiscip. Rev. Comput. Mol. Sci.* **2011**, *1*, 211–228. [CrossRef]

47. Credendino, R.; Minenkov, Y.; Liguori, D.; Piemontesi, F.; Melchior, A.; Morini, G.; Tolazzi, M.; Cavallo, L. Accurate experimental and theoretical enthalpies of association of TiCl4 with typical Lewis bases used in heterogeneous Ziegler-Natta catalysis. *Phys. Chem. Chem. Phys.* **2017**, *19*, 26996–27006. [CrossRef]

48. Dolg, M.; Wedig, U.; Stoll, H.; Preuss, H. Energy-adjusted abinitio pseudopotentials for the first row transition elements. *J. Chem. Phys.* **1987**, *86*, 866–872. [CrossRef]

49. Partin, D.E.; O'Keeffe, M. The structures and crystal chemistry of magnesium chloride and cadmium chloride. *J. Solid State Chem.* **1991**, *95*, 176–183. [CrossRef]

50. Frisch, M.J.; Trucks, G.W.; Schlegel, H.B.; Scuseria, G.E.; Robb, M.A.; Cheeseman, J.R.; Scalmani, G.; Barone, V.; Mennucci, B.; Petersson, G.A.; et al. *Gaussian 09, Revision B.01.*; Gaussian, Inc.: Wallingford, CT, USA, 2010.

51. Corradini, P.; Guerra, G. Models for the stereospecificity in homogeneous and heterogeneous Ziegler-Natta polymerizations. *Prog. Polym. Sci.* **1991**, *16*, 239–257. [CrossRef]

52. Corradini, P.; Guerra, G.; Cavallo, L. Do New Century Catalysts Unravel the Mechanism of Stereocontrol of Old Ziegler−Natta Catalysts? *Acc. Chem. Res.* **2004**, *37*, 231–241. [CrossRef]

53. Busico, V.; Corradini, P.; De Martino, L.; Proto, A.; Savino, V.; Albizzati, E. Polymerization of propene in the presence of MgCl2-supported Ziegler-Natta catalysts, 1. The role of ethyl benzoate as "internal" and "external" base. *Makromol. Chem.* **1985**, *186*, 1279–1288. [CrossRef]

54. Credendino, R.; Busico, V.; Causà, M.; Barone, V.; Budzelaar, P.H.M.; Zicovich-Wilson, C. Periodic DFT modeling of bulk and surface properties of MgCl2. *Phys. Chem. Chem. Phys.* **2009**, *11*, 6525–6532. [CrossRef] [PubMed]

55. Breuza, E.; Antinucci, G.; Budzelaar, P.H.M.; Busico, V.; Correa, A.; Ehm, C. MgCl2-Supported Ziegler–Natta Catalysts: A DFT-D "Flexible-Cluster" Approach to Internal Donor Adducts. *J. Phys. Chem. C* **2018**, *122*, 9046–9053. [CrossRef]

56. Ratanasak, M.; Rungrotmongkol, T.; Saengsawang, O.; Hannongbua, S.; Parasuk, V. Towards the design of new electron donors for Ziegler–Natta catalyzed propylene polymerization using QSPR modeling. *Polymer* **2015**, *56*, 340–345. [CrossRef]

57. Kim, G.-H.; Um, B.-H.; Son, K.-C.; Oh, K.; Koh, H.-L. MgCl2-supported Ziegler–Natta catalyst containing dibenzoyl sulfide donor for propylene polymerization. *J. Appl. Polym. Sci.* **2014**, *131*, 40743–40748. [CrossRef]